the Doppler shift, 0.25 Å, exceeds the width of the solar OI lines as recently observed at high resolution by groups from the Naval Research Laboratory (*7*) and the University of Colorado (*8*). Resonance scattering from the solar continuum and fluorescence excited by Lyman β (*9*) contribute roughly equally to the OI *g*-factor given in Table 1. For the CI line at 1657 Å, high-resolution solar spectra (*7*) were used to compute the *g*-factor given. Because of the multiplet structure of this line, the Doppler-shifted value is only reduced by a factor of 2 from the unshifted one.

The *g*-factors and lifetimes (*10*) at 1 A.U. adopted for this work and the derived values of the source rate Q are also given in Table 1. The error in the Q values is due principally to the uncertainties in both *g*-factors and lifetimes and may well exceed a factor of 2. The Q value for H, also given in Table 1, is obtained by scaling the production rate derived by Opal *et al.* (*2*) from the Lyman α isophotes and our maximum apparent Lyman α brightness of 60 kR integrated over the field of view (7 by 35 arc minutes). Alternative values for H, based on the solar Lyman α flux (average inner blue wing) derived by Keller and Thomas (*11*) from an analysis of the curvature of the Lyman α coma of Comet Bennett, are also given. The actual value of Q_{H} most likely lies somewhere between the two values given in Table 1.

Despite the high probable errors in the source rates given in Table 1, these results present a consistent picture of water vapor dissociation in which

$$Q_{\mathrm{H_2O}} = Q_{\mathrm{O}} = Q_{\mathrm{OH}} = \frac{1}{2} Q_{\mathrm{H}}$$

Moreover, it is clear that atomic carbon is produced at about the same rate as water vapor, and this can occur only if the parent molecule containing the carbon is evaporated at the same rate as H_2O. Delsemme (*12*) has pointed out that production rates of C_2 or CN are typically of the order of 1 percent of the water production rate for a "medium-bright" comet such as Comet Bennett, so it is unlikely that any hydrocarbon molecule is the carbon parent. This points to CO as the probable source of the carbon, and the limit on Q_{CO} set by the data on the CO fourth positive system is consistent with Q_{C}. While CO_2 is also a likely candidate and cannot be excluded by the data on the production rate of CO_2 set by the CO_2^+ doublet, the large strength of CO^+ bands usually observed in comet tails, relative to the strength of CO_2^+ bands, argues strongly for CO as the parent molecule. The view is further supported by the fact that CO is observed to be the second most abundant molecule, after H_2, in the interstellar medium (*13*).

PAUL D. FELDMAN
PETER Z. TAKACS
WILLIAM G. FASTIE
Physics Department,
Johns Hopkins University,
Baltimore, Maryland 21218
BERTRAM DONN
Astrochemistry Branch,
NASA Goddard Space Flight Center,
Greenbelt, Maryland 20771

References and Notes

1. A. D. Code, T. E. Houck, C. F. Lillie, *NASA SP-310* (1972), p. 109.
2. C. B. Opal, G. R. Carruthers, D. K. Prinz, R. R. Meier, *Science* **185**, 702 (1974).
3. A. Dalgarno and T. C. Degges, *Planetary Atmospheres, Proc. IAU (Int. Astron. Union) Symp. No. 40* (1971), p. 337.
4. C. A. Barth, *Appl. Opt.* **8**, 1295 (1969).
5. G. L. Siscoe and N. R. Mukherjee, *J. Geophys. Res.* **77**, 6042 (1972); W. I. Axford, *NASA SP-308* (1972), p. 609.
6. M. B. McElroy and D. M. Hunten, *J. Geophys. Res.* **75**, 1188 (1970); M. B. McElroy and J. C. McConnell, *ibid.* **76**, 6674 (1971).
7. G. E. Brueckner and K. Nicolas, *Bull. Am. Astron. Soc.* **4**, 378 (1972).
8. E. C. Bruner, Jr., R. W. Parker, E. Chipman, R. Stevens, *Astrophys J. Lett.* **182**, L33 (1973).
9. T. M. Donahue and W. G. Fastie, in *Space Research 4*, P. Muller, Ed. (North-Holland, Amsterdam, 1964), p. 304.
10. The OH lifetime is taken from measurements on Comet Kohoutek (1973f) by J. Blamont and M. Festou [*C. R. Hebd. Seances Acad. Sci. Ser. B Sci. Phys.* **278**, 479 (1974)]. The OH *g*-factor, allowing for a Doppler shift of 55 km sec^{-1}, is from F. Mies (private communication).
11. H. U. Keller and G. E. Thomas, *Astrophys. J. Lett.* **186**, L87 (1973).
12. A. H. Delsemme, *Space Sci. Rev.* **15**, 89 (1973).
13. D. M. Rank, C. H. Townes, W. J. Welch, *Science* **174**, 1083 (1971).
14. We wish to acknowledge the excellent support given by the Sounding Rocket Division of NASA Goddard Space Flight Center and the Naval Ordnance Missile Test Facility at White Sands Missile Range during the preparation and launch of this experiment. We thank C. B. Opal and K. Nicolas for valuable discussions. This work was supported by NASA grant NGR 21-001-001.

22 April 1974

Meteors and Meteorites Detected by Infrasound

Abstract. *The Lamont-Doherty tripartite array of microphones has detected acoustic signals from meteors. These signals yield trace velocities which vary rapidly from supersonic to nearly infinite values for successive waves or wave groups, indicating a rapidly moving source. The trajectory is constructed on the basis of an assumption of reasonable path elevations. With a second array it would be possible to obtain more positive trajectory fixes and probable ground impact locations. Initial results suggest that most acoustic meteors are meteorite-type objects rather than the low-density objects commonly detected at high elevations by photographic and radio techniques.*

The Lamont-Doherty infrasound system consists of two tripartite arrays of capacitor microphones at the same location operating in the passbands 0.1 to 1 hertz and 1 to 10 hertz, respectively. The horizontal trace velocity and the source azimuth are computed from the differences in the arrival times of the waves across each array. Many signals have been recorded which we attribute to meteoric sources.

Table 1. Data computed for waves 1 through 10 from observations of wave arrival times at the tripartite elements.

Wave number	Azimuth (deg)	Trace velocity (m/sec)	Elevation angle (deg)
1	148	391	28
2	157	500	47
3	158	600	55
4	161	650	58
5	168	840	66
6	200	990	69
7	236	1140	73
8	263	1140	73
9	274	950	68
10	290	800	65

An example of a typical signature of meteoric infrasound is shown in Fig. 1A, which indicates how such signals stand out from the background. The pressure amplitudes of the meteor signatures are about 1 μbar (1 dyne/cm^2). Figure 1B is a tape playback of the acoustic signal to a strip chart driven at high speed. Similar phases are correlated wtih broken lines. For the more common stationary acoustic sources, the slopes would be constant, indicating a constant time delay across the array. But here the slopes show a rapidly changing and decreasing time delay to nearly zero between waves 6 and 7 and then a reverse in direction with increasing delay. Such rapidly changing time delays indicate a fast-moving elevated source. For an airplane to generate the observed signal at a normal cruising elevation, about

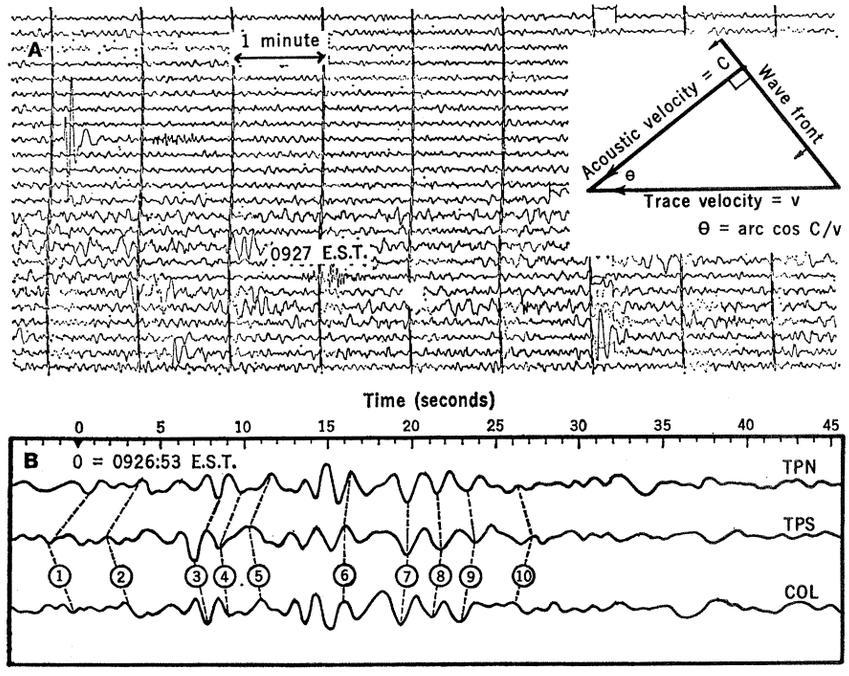

Fig. 1. (A) Portion of the 24-hour visual drum record from a sensitive microphone for 20 October 1973. The high-frequency acoustic meteor signal at 0927 E.S.T. stands out clearly against the background pressure noise, due mostly to local wind. Time marks are at 1-minute intervals. (B) Tape playback to a high-speed recorder of the acoustic signal in (A). Lines correlate the same phases (for identical waves numbered 1 through 10) among the records from the three instruments of our tripartite array (TNP, TPS, and COL). The inset in (A) explains the relationship between the horizontal acoustic trace velocity and the actual ray path and indicates how the elevation angle is calculated.

10 km, a velocity at least three times the speed of sound would be required to satisfy the observations; moreover, an airplane would generate a single N-wave oscillation, not a prolonged train of waves.

From the horizontal trace velocities calculated from wave phase differences (as the waves cross our array) and local acoustic speeds we have computed the source elevation angle θ for each wave (see Fig. 1A, inset). Table 1 shows the azimuths, trace velocities, and elevation angles computed for waves 1 through 10. To obtain space "fixes" for the meteor trajectory a minimum of two tripartite arrays is necessary. One determines the orientation of the horizontal projection of the trajectory by assuming some constant arbitrary elevation h (50 km) of the trail and then computing the horizontal distance x for each wave with the use of h and θ from the formula

$$x = h/\tan\theta$$

We can construct a more refined trajectory on the basis of assumed upper and lower elevations of the true trail. In this construction we assume that the acoustic wave train consists of a simple series of waves following progressively increasing travel times from the closest to the farthest points on the trajectory. We also ignore possibly appreciable effects of wave refraction and interference.

Moreover, in view of the nearly infinite velocity of the meteor relative to the speed of sound, it can be easily deduced that the order of wave arrival depends on the position of the meteor trail relative to the observer. The first wave to arrive may thus come from any part of the trajectory. In the present case the acoustic waves appear to emanate in sequence from the end to the beginning of the trail. According to Krinov (*1*), shock waves will not be generated until the meteor penetrates to an elevation of 60 to 80 km. On the basis of our experience with rocket infrasound and the fact that wave 10 probably does not represent the first acoustic wave generated, we selected 55 km as a reasonable source elevation for this wave. Because meteors decelerate to subsonic speeds below about 20 km [for example, see Hawkins (*2*)] we selected 25 km as the source elevation for wave 1.

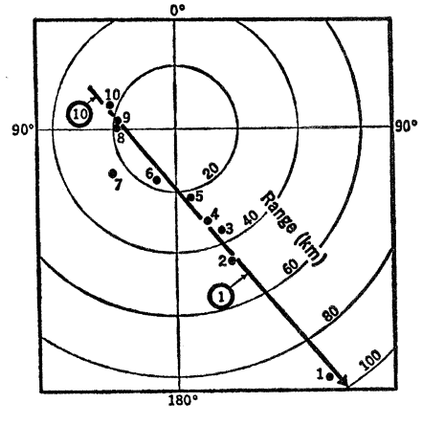

Fig. 2. Horizontal projection of the trajectory of the acoustic source of the signal in Fig. 1 constructed on the basis of a constant elevation of 50 km. The short numbered arrows indicate the points of origin for waves 1 and 10 (in Fig. 1), assuming source elevations of 25 and 55 km, respectively.

With these elevations and the data from Table 1, we have located the sources of waves 1 and 10 on the trajectory (see the circled numbers in Fig. 2). The spacing between waves 1 and 10 will contract considerably if wave refraction is considered.

From this information we can compute the time duration of waves 1 through 10 as a rough test of procedure. The distances traveled by waves 1 and 10 are computed from the given data to be 53 and 61 km, respectively. For a mean acoustic speed of 300 m/sec, we obtain travel times of 176 and 203 seconds, respectively, for waves 1 and 10. The difference of 27 seconds is in good agreement with the measured arrival time difference of 26 seconds between waves 1 and 10 in Fig. 1B. The irregularity in the wave amplitudes is probably due to some combination of source variations, propagation effects, and interference caused by waves from different parts of the meteor trail.

A second array at another location would provide the additional data necessary for a more reliable acoustic determination of the wave trail in space. This procedure has the further value of making possible a calculation of a fairly accurate fix for fallen bodies. More accurately, the procedure would give a fix for the body at its last point of supersonic flight. According to Krinow (*1*) and Hawkins (*2*), this occurs in the lower stratosphere where atmospheric drag terminates the cosmic component of motion; from this point on, gravitational free fall becomes the form of motion. By this

procedure we would thus be able to locate the atmospheric "epicenter" of the impact point.

So far we have analyzed only a dozen signals in the detail shown for the case described here. But a survey of 8 years of visual drum recordings reveals a strong minimum of occurrence in the hours between midnight and dawn. These observations seem to match the 3 a.m. minimum shown in the diurnal distribution of meteor falls given by Heide (*3*); we realize, of course, that the existence of such a nocturnal minimum may in part be due to a nocturnal absence of observers. Heide explains this minimum (if real) as a meteor velocity effect due to the earth's orbital speed (about 30 km/sec). The high speed resulting from the combination of the approach of an early-morning meteor with the orbital speed of the earth would cause complete destruction of the meteor in the high atmosphere. Lower resultant speeds, especially for meteors arriving later in the day, would permit them to fall or at least to reach elevations low enough to shock the atmosphere, thus generating acoustic waves.

From this information and our analysis it appears that the objects we have detected belong to the class of more dense, meteorite-type bodies rather than to the class of "fluffy" or "dust ball" objects detected more commonly by photographic and radio means at elevations between 80 and 100 km. The acoustic method may thus provide a means for estimating the flux of sporadic, meteoritic material rather than that of the less dense upper-atmospheric meteoric bodies. For flux determinations, a grid of single-site acoustic detectors is necessary with one of the sites being tripartite to permit distinctions to be made between the meteoric signals and stationary artificial sources.

Finally, the dominant recorded energy for these wave trains lies within 0.3 to 3 hertz. The low-frequency cutoff is sharp, being a function of source parameters; the higher-frequency portion falls gradually, being a function of attenuation effects.

WILLIAM L. DONN
Lamont-Doherty Geological Observatory of Columbia University, Palisades, New York 10964, and *City College of New York, New York 10031*
NAMBATH K. BALACHANDRAN
Lamont-Doherty Geological Observatory of Columbia University

References and Notes

1. E. L. Krinov, in *Principles of Meteoritics* (translated by I. Vidziunas), H. Brown, Ed. (Pergamon, London, 1960).
2. G. S. Hawkins, *The Physics and Astronomy of Meteors, Comets, and Meteorites* (McGraw-Hill, New York, 1964).
3. F. Heide, *Meteorites* (translated by E. Anders and E. DuFresne) (Univ. of Chicago Press, Chicago, 1957).
4. This work was supported by grant GA 33710X from the National Science Foundation, grant DA-AROD-71-G-90 from the Army Research Office, Durham, North Carolina, and contract DAAB-07-74-C-0045 from the U.S. Army Electronics Command, Fort Monmouth, New Jersey. Lamont-Doherty Geological Observatory of Columbia University contribution No. 2127 and City University of New York, University Institute of Oceanography, contribution No. 34.

15 April 1974; revised 20 May 1974

Transformation of Chick Embryo Neuroretinal Cells by Rous Sarcoma Virus in vitro: Induction of Cell Proliferation

Abstract. *Neuroretinal cells from 7-day-old chick embryos are transformed and induced to proliferate after infection with Rous sarcoma virus in vitro. Susceptibility of neuroretinal cells to the virus is also dependent on the stage of development since infection of cells from 10-day-old embryos is uneffective.*

Interactions of Rous sarcoma virus (RSV) with permissive cells in vitro have been mainly studied in chick embryo fibroblasts. Cells from differentiated chick tissues, such as iris epithelium (*1*) and myoblasts (*2*), can also be transformed by RSV and release virus. However, no chick cells from a neural tissue have been shown to be susceptible in vitro to infection and transformation by RSV.

We report that RSV infection of neuroretinal (NR) cells from 7-day-old chick embryos in vitro results in morphological transformation and virus replication. The transformed NR cells were induced to proliferate up to 12 doublings. In contrast, NR cells from 10-day-old embryos were not transformed by RSV, supported only minimal virus replication and did not multiply. Neuroretina was selected for these experiments since this tissue is made exclusively of neural cells and has a low capacity for multiplication in vitro (*3*). Neuroretinas were dissected from leukosis-free flocks of brown Leghorn chick embryos after fertile eggs were incubated for 7 or 10 days at 37°C. The tissues were dissociated as described (*4*), and the yield of cells ranged from 4×10^6 cells (7-day embryos) to 4×10^7 cells (10-day embryos) per neural retina. Cultures obtained by this procedure consisted mainly of small, round cells with an average diameter of 6 μm and were entirely devoid of pigmented cells and fibroblasts. A high titer variant of the Schmidt Ruppin strain of RSV, subgroup D, was used in our experiments. The virus was produced and assayed on fibroblasts from brown Leghorn chick embryos of the C/O phenotype as judged by their susceptibility to the four main subgroups of avian oncornaviruses. Suspensions of single NR cells, in Eagle's minimal essential medium supplemented with 5 percent calf serum, 10 percent Bacto tryptose phosphate, and antibiotics were infected with RSV at a multiplicity of about one focus-forming unit (FFU) per cell, in the presence of diethylaminoethyl dextran (5 μg/ml) (*5*). Portions (2×10^6) of control or infected cells were seeded in 35-mm plastic petri dishes and kept at 37°C in a humidified atmosphere (5 percent CO_2 in air). Complete cell attachment occurred within 2 hours. The medium (2 ml per dish) was renewed the following day and every third day thereafter.

Table 1. Kinetics of RSV replication in NR cells from 7- and 10-day chick embryos. Infected NR cells (2×10^6) in 2 ml of Eagle's minimal essential medium containing 5 percent calf serum and 10 perecnt Bacto tryptose phosphate were seeded in 35-mm plastic petri dishes. Four hours later, attached cells were extensively washed to eliminate unadsorbed virus. Fresh medium (2 ml) was added and renewed at intervals as indicated. RSV was titrated by the focus-forming assay on chick embryo fibroblasts of the C/O phenotype.

Time after infection	Virus titers (FFU/ml) in NR cells from	
	7-day embryos	10-day embryos
Day 0*	2×10^6	2×10^6
Day 1	2×10^3	30
Day 3	7×10^4	9
Day 5	7×10^5	
Day 6	1.2×10^6	
Day 8	3×10^6	50

* Input virus.

Morphological transformation was evident in NR cells from 7-day embryos within 36 hours after infection by RSV and simultaneously affected most of the